MAGNETIC CIRCUIT MODELING OF THE HALL EFFECT CURRENT SENSOR

Bui Anh Tuan[1,*], Nguyen Tien Dung[2]

DOI: https://doi.org/10.57001/huih5804.2026.110

ABSTRACT

This paper presents an equivalent magnetic circuit modeling approach for closed-loop Hall-effect current sensors to address the computational inefficiencies of conventional numerical simulations. A key contribution of this research is the integration of the Jiles-Atherton hysteresis model with flux tube elements, enabling a rigorous analysis of nonlinear phenomena, including leakage flux and magnetic core saturation, over a wide frequency bandwidth (200 Hz to 200kHz). The proposed methodology employs the Nelder-Mead Simplex algorithm to optimize sensor geometries, ensuring accurate magnetic field distribution modeling while bypassing the need for computationally intensive finite element analysis. Experimental validation conducted on ABB commercial sensors (ES300 to ES2000 series) demonstrates high fidelity, with a maximum root-mean-square error of approximately 6%. This study provides a robust design tool for predicting sensor performance and optimizing magnetic materials in modern power electronics applications. The model effectively balances physical accuracy with the high computational speed required for real-time simulation environments.

Keywords: *Magnetic Hysteresis, Hall effect current sensor, Jiles-Atherton model, Flux tubes model, Magnetization circuit simulation*

[1]Faculty of Electrical and Electronic Engineering, Thuyloi University, Vietnam
[2]Faculty of Control and Automation, Electric Power University, Vietnam
[*]Email: tuanba@tlu.edu.vn
Received: 03/3/2026
Revised: 05/5/2026
Accepted: 25/5/2026

1. INTRODUCTION

In modern power electronic systems, closed-loop Hall effect current sensors play a pivotal role due to their high measurement accuracy, wide bandwidth, and excellent electrical isolation. However, the design and optimization of these devices face significant challenges arising from the complex interaction between electronic components on the circuit board and the non-linear characteristics of the magnetic circuit [1].

The main parts of the Hall effect current sensor are shown in Figure 1. The primary current, passing through the sensor, creates a magnetic field channeled by the magnetic circuit. The magnetic flux is directed toward the air gap, where a Hall effect probe is placed, delivering a voltage proportional to the magnetic induction. The electronic board converts this voltage into a secondary current, which must, at all times, be proportional to the primary current and the number of primary and secondary turns (and respectively), according to equation (1):

$$N_p I_p + N_s I_s = 0 \quad (1)$$

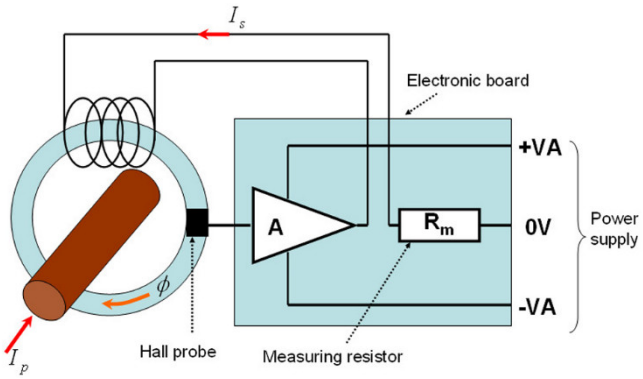

Figure 1. Main parts of the Hall effect current sensor

In practice, a complete sensor consists of two distinct yet closely linked parts:

The electronic board: Comprising a vast number of components such as transistors, diodes, resistors, and capacitors. The analysis of this part is typically performed effectively using dedicated circuit simulation software.

The magnetic circuit: Where complex physical phenomena occur, such as leakage flux, the fringing effect at the air gap, and core saturation.

The greatest challenge for engineers today is the lack of a magnetic circuit model that ensures both high physical accuracy (similar to Finite Element Analysis - FEA)

and sufficient flexibility for direct integration into circuit simulation software for comprehensive system analysis [2]. Previous studies have often overlooked virtual geometric parameters or failed to provide a unified identification protocol for various device series [3-5].

This paper proposes a novel approach by developing a Magnetic Equivalent Circuit (MEC) model based on flux tube theory and the Jiles-Atherton hysteresis model [6, 7]. The core of this research is to establish an identification protocol for key geometric parameters to accurately reflect non-linear phenomena. The effectiveness of this protocol is validated through its application to a range of commercial sensors from the ABB Group, including the ES300, ES500, ES1000, and ES2000. The results not only help clearly position the study within the context of existing solutions but also provide a powerful tool for predicting sensor behavior under harsh operating conditions.

2. MAGNETIC CIRCUIT MODELING OF THE SENSOR

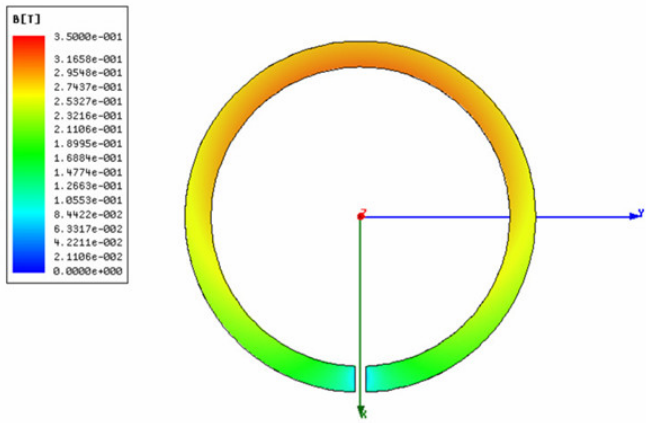

Figure 2. Magnitude of the magnetic induction in the magnetic circuit for $N_pI_p = 80A$

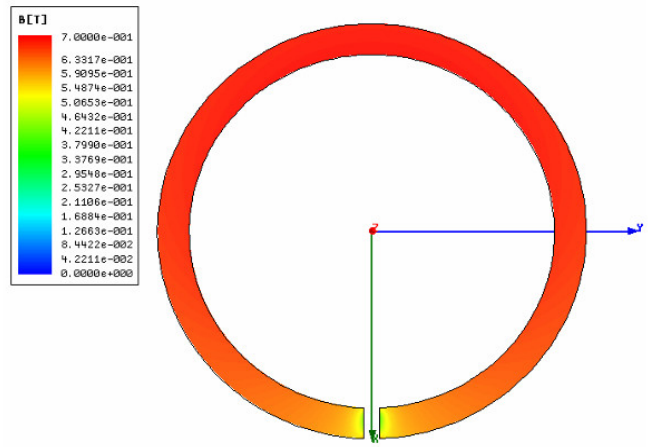

Figure 3. Magnitude of the magnetic induction in the magnetic circuit for $N_pI_p = 800A$

As we have seen in the diagram in Figure 1, the sensor's magnetic circuit includes an air gap. This air gap causes magnetic flux leakage, which prevents the magnetic quantities from being considered homogeneous along the perimeter of the magnetic circuit. To account for this effect, 3D finite element simulations were performed in magnetostatics using the MAXWELL software [5].

Figures 2 and 3 show the magnitude of the magnetic induction for two different current levels. Figure 2 shows that the magnetic induction is higher on the side opposite the air gap over nearly half of the toroid. This phenomenon is accentuated if the material is saturated, as shown in Figure 3. To account for magnetic leakage, we propose modeling the magnetic circuit using an equivalent magnetic circuit with the topology presented in Figure 4.

In the diagram of Figure 4, the elements and quantities involved are:

R_1, R_2, R_3: Flux tubes of the toroidal magnetic circuit

R_{leak}: Flux tube representing leakage

R_{ag}: Flux tube representing the air gap

N1.I, N2.I, N3.I: Fictitious magnetomotive force sources such that $N1+N2+N3 = N_p$

Φ_1, Φ_2, Φ_3: Branch magnetic fluxes

After analysis, to correctly represent leakage effects, the specific parameters that cannot be identified analytically have been reduced to three.

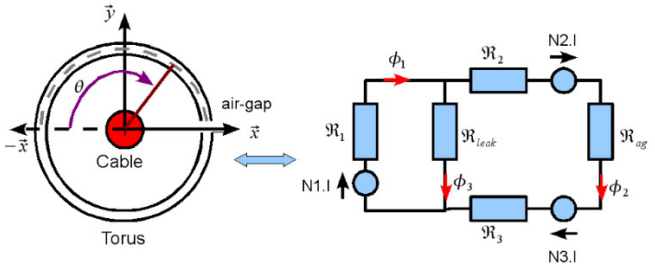

Figure 4. Topology of the equivalent magnetic circuit

These parameters are:

- α: the angular position of the leakage flux tube;
- S_{ag}: the cross-section of the air-gap tube;
- S_{leak}: the cross-section of the leakage tube.

We identify these parameters using an optimization algorithm [8]. The objective function, equation (2), is defined here as the normalized mean distance between the induction curves calculated by 3D finite element methods (B_{3DFE}) and those calculated by the equivalent

magnetic circuit (B_{MEC}) as a function of the angular position θ (see Figure 4), along the perimeter of a half magnetic circuit and a half air-gap, n represents the number of points on the curve:

$$OF_i=\frac{100}{n}\sum_{k=1}^{n}\sqrt{\left(\frac{B_{3DFE}(k)-B_{MEC}(k)}{\max(B_{3DFE})}\right)^2} \quad (2)$$

In order to find constant parameters (independent of the current level) and to achieve a compromise between linear behavior (low N_pI_p) and saturated behavior (high N_pI_p), two objective functions are evaluated (OF1 for low N_pI_p and OF2 for high N_pI_p). Then, these two objective functions are combined into one to obtain a single objective (equation (3)):

$$OF=\sqrt{OF_1^2+OF_2^2} \quad (3)$$

The optimization results are shown in Figure 5. An angular position of 180° corresponds to the center of the air gap.

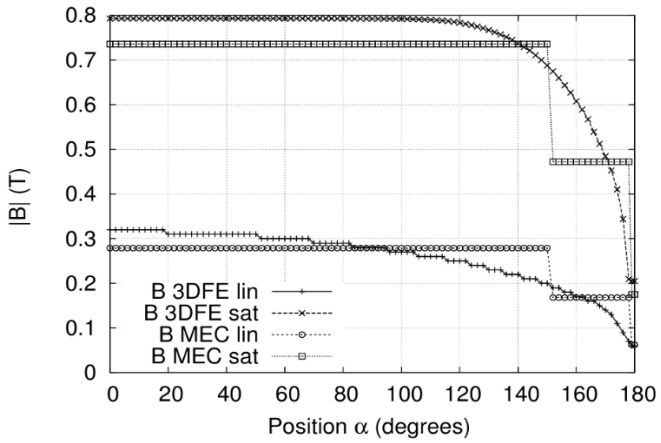

Figure 5. Magnetic induction magnitude along a half magnetic circuit and air gap. (MEC: Magnetic Equivalent Circuit, 3DFE: 3D Finite Elements, lin: low N_pI_p, sat: highN_pI_p)

Figure 5 shows that the curve of the induction magnitude calculated by the magnetic equivalent circuit (MEC) is a "staircase-shaped" curve. The first part of the MEC curves (from 0° to 150°) represents the induction in R_1. The second part (from 151° to 178°) represents the induction in R_2, and the final part is the induction in the air gap. After identification, the three parameters α, k_1 and k_2 are reported in Table 1 for all sensor types. k_1 and k_2 are coefficients such that $k_1 = S_{leak}/S_{MC}$ and $k_2 = S_{ag}/S_{MC}$, where S_{MC} is the cross-section of the magnetic circuit.

It can be observed in Table 1 that $k_2 > 1$. which can be explained by the fringing of the field lines in the air gap. As the magnetic flux passes through the air gap. it does not travel in a straight line but spreads out. causing the effective flux area to be larger than the physical cross-section of the magnetic core. Similarly. $k_1 >> 1$. so as to represent all leakage lines as a single flux tube. For most ABB sensors. the angle α ranges from 138° to 150° (near the air gap). Notably. the ES300 model has an angle of α = 94°. indicating a difference in the mechanical structure or material properties of this specific series.

Table 1. Parameter values for each sensor type

ES	α (degrees)	k_1	k_2	OF
300	94	47	3.53	1.99
500	150	33	2.7	1.43
1000	150	44	3.67	1.61
2000	138	53	3.32	1.51

3. VALIDATION OF THE MAGNETIC MODELING

To validate the magnetic modeling. we first disconnect the electronic board. and the measuring resistor is directly connected to the secondary winding. The primary current I_p is supplied by an inverter. I_p is measured using a shunt and I_s is measured via the voltage across the measuring resistor. The I_p signal. measured and recorded in a text file. is then directly imposed onto the simulation. and we compare the measured and simulated I_s values. To simulate the magnetization circuit. several simulation models can be applied. such as: the dynamic flux tube with the Dynamic Static Feedback (DSF) model associated with the Jiles-Atherton static model. and the dynamic flux tube with the Dynamical with Wall Motion (DWM) model [6, 7, 9]. Figure 6 illustrates the simulation schematic of the magnetization circuit using the dynamic flux tube with the DSF model associated with the Jiles-Atherton static model. developed in Matlab-Simulink.

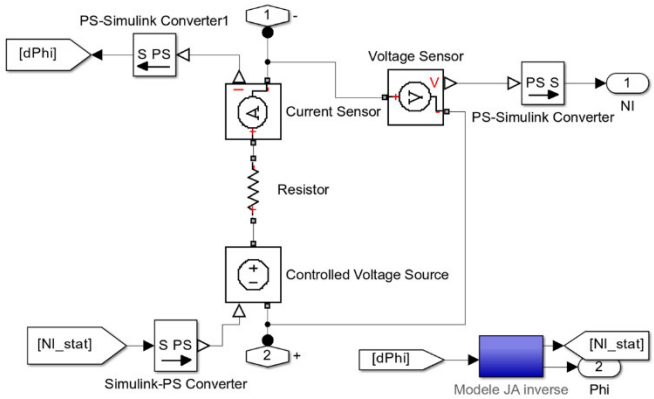

Figure 6. Simulation model of the current sensor magnetization circuit

Several levels of current and different frequencies were tested on each type of sensor. We present here

those that seem most representative to us. Figures 7, 8 show the measured and simulated secondary currents I_s for the ES1000 sensor. for a sinusoidal I_p signal with an RMS value of I_p = 1000A and for frequencies of f = 5Hz, f = 20Hz and f = 200Hz respectively.

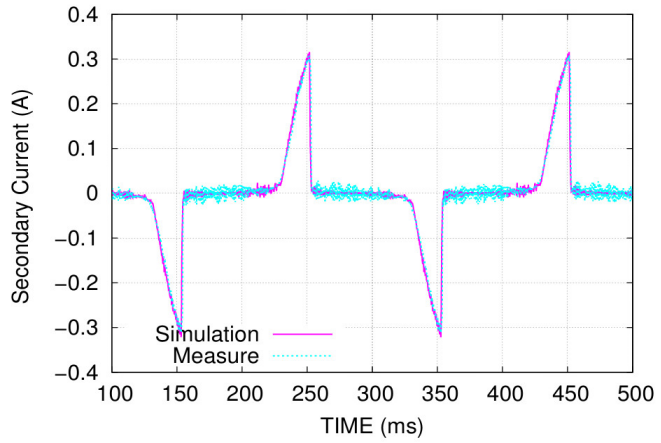

Figure 7. Comparison of measured and simulated secondary currents for $I_p = 1000A_{RMS}$, f = 5Hz

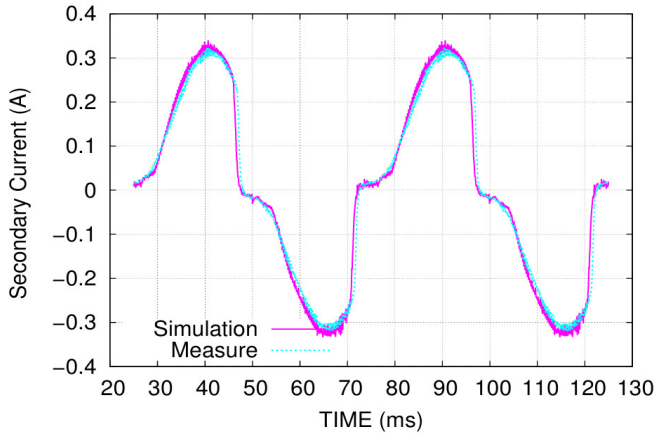

Figure 8. Comparison of measured and simulated secondary currents for $I_p = 1000A_{RMS}$, f = 20Hz

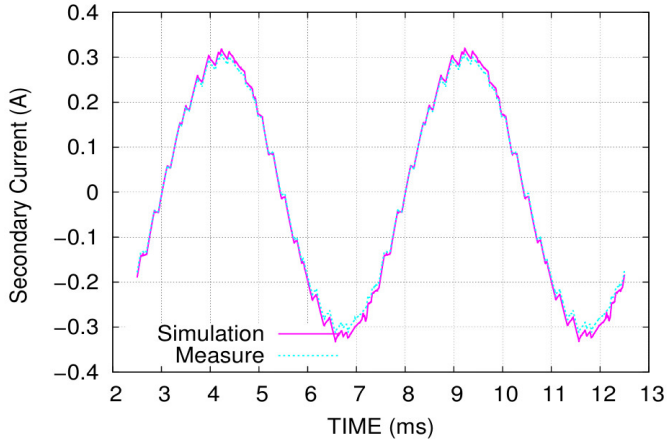

Figure 9. Comparison of measured and simulated secondary currents for $I_p = 1000A_{RMS}$, f = 200Hz

Figures 7 and 8 show that at low frequencies. the magnetic material saturates because the voltage generated at the secondary does not create sufficient current to compensate for the primary ampere-turns. This induces distortions in the secondary current. This behavior is perfectly captured by our model. At higher frequencies (Figure 9). the distortions disappear. We can also observe in Figure 8 that. since the measured primary current signal is directly imposed onto the simulation. the inverter switching transitions on the primary current can be seen in the secondary current.

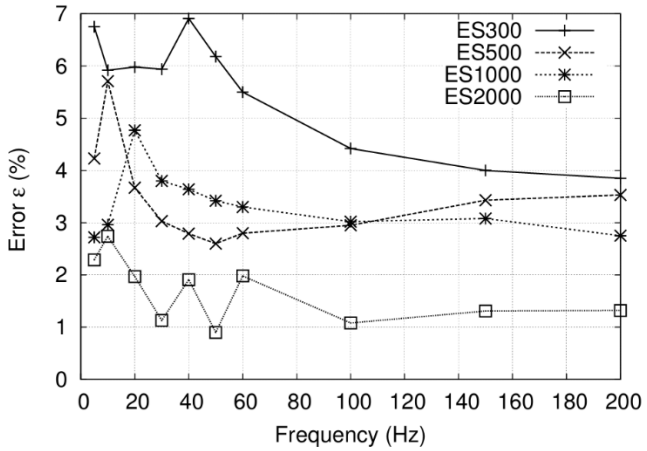

Figure 10. Variations of ε as a function of frequency for each sensor type

The accuracy of the simulation results between the measured secondary current and the simulated secondary current is estimated by the quadratic error ε. Figure 10 shows the variations of ε as a function of frequency for each sensor type. It can be observed that ε is of the same order of magnitude for all sensor types and remains relatively constant over a wide range of frequencies. The higher errors at low frequencies can be explained by the fact that during distortions. the signals are highly noisy. which may introduce additional error.

4. COMPLETE SYSTEM VALIDATION

We will now add to the model the electronic board used to regulate the secondary current so that it reflects the primary current [10, 11]. Figures 11 and 12 show the primary currents referred to the secondary. as well as the measured and simulated secondary currents. for an ES300 type sensor in two different situations. On the left. the electronic board is not connected (same situation as before); on the right. the electronic board is connected. and the input signal is identical to the one in the left figure.

As shown in Figures 11 and 12, the implemented model accurately reproduces the measured secondary

current regardless of the conditions (high current. low frequency. electronic board connected or not). The electronic board. including all its components. does not interfere with the simulation. In fact. it can even improve the computation time in certain cases. Indeed. the saturation of the magnetic circuit induces strong non-linearities that force the solver to reduce its time step when operating in that region. Under regulated operation. this situation is avoided. and this pitfall is bypassed. Although there are more components to simulate. the solver is much better suited to this type of scenario.

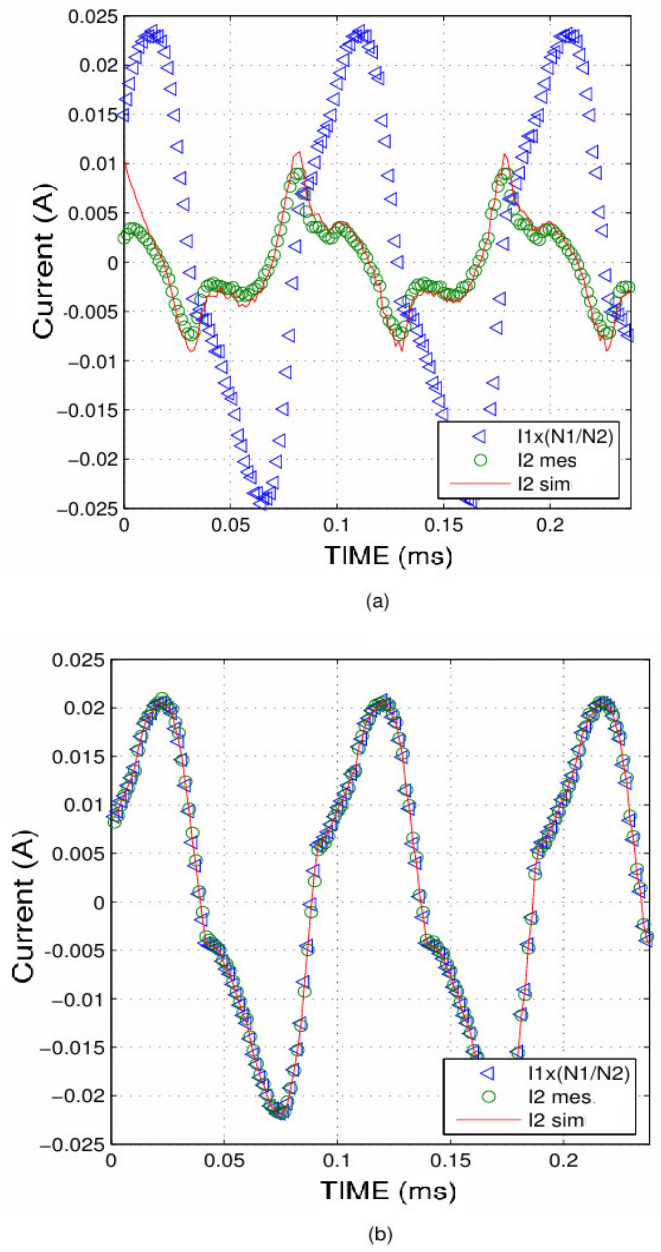

Figure 11. Unregulated operation (a) and regulated operation (b) for a test at I_{max} = 40A and f = 10Hz

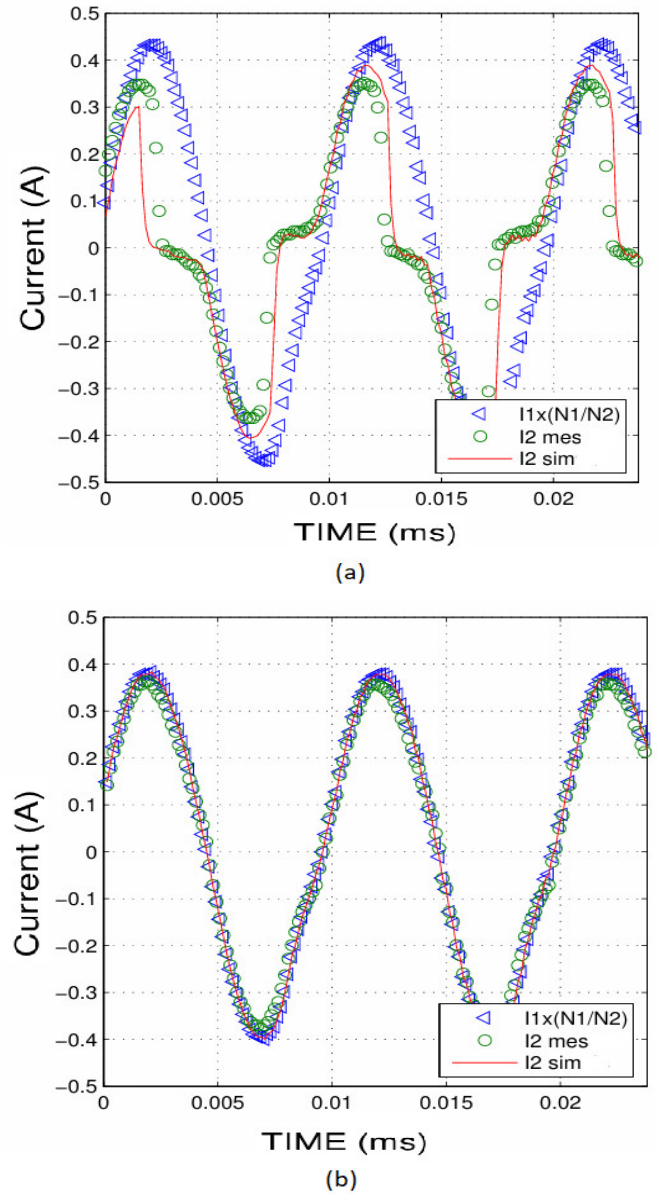

Figure 12. Unregulated operation (a) and regulated operation (b) for a test at I_{max} = 800A and f = 200Hz

Table 2. Root mean square error across various current and frequency values

Test No.	f (Hz)	I_1 (A)	Error (%)
1	10	40	1.84
2	50	350	1.02
3	100	750	2.86
4	500	750	5.68
5	1000	500	6.12
6	2000	300	1.67

Table 2 presents the percentage root mean square error between the measured and simulated secondary currents for various tests. These tests focused on

regulated operation. as it is the most relevant scenario and best reflects the sensor's real-world performance.

As seen in Table 2, the model accurately predicts the simulated secondary current. with the error reaching 6% at most.

5. CONCLUSION

The paper proposes an optimization method to develop an equivalent magnetization circuit model for Hall effect current sensors. The effectiveness of this model is compared and evaluated against experimental results across various current levels and operating frequencies. with a maximum square error of approximately 6%. The combination of the magnetization circuit model and the electronic board model allows for an accurate reproduction of the secondary current response under different operating conditions. Consequently. this provides an efficient solution for the design and analysis of ABB current sensors (ES300-ES2000).

Based on the confidence index obtained from validating the model against real current sensors. we will perform virtual testing with common electrical engineering materials. The objective is to verify whether our model is capable of identifying the best material to replace the existing magnetic materials currently used in these current sensors.

REFERENCES

[1]. Marco Crescentini, Sana Fatima Syeda, Gian Piero Gibiin, "Hall-Effect Current Sensors: Principles of Operation and Implementation Techniques," *IEEE Sensors Journal*, 22:10137-10151, 2022.

[2]. Brahim Ladghem Chikouche, Kamel Boughrara, Frédéric Dubas, Rachid Ibtiouen, "Two-dimensional hybrid model for magnetic field calculation in electrical machines: Exact subdomain technique and magnetic equivalent circuit," *COMPEL.*, 40(3): 535-560, 2021.

[3]. S Wang, F Chen, Z Tian, X Wu, "An enhanced magnetic equivalent circuit model for a magnetorheological clutch including nonlinear permeability. flux fringing. and leakage effects," *IEEE Transactions on Transportation Electrification*, 9(1): 488 - 500, 2022.

[4]. Xingjian Zhao, Li Jiang, Ge Gao, Hong Lei, "Study on the Influence of Strong Background Magnetic Field on Hall Current Sensors and Mitigating Strategies," *IEEE Transactions on Instrumentation and Measurement*, 74:1-11, 2025.

[5]. Fan H., Li S., Cen Y., Feng Q., Heidari H., "A Horizontal Hall Sensor 3D COMSOL Model," in *IEEE 63rd International Midwest Symposium on Circuits and Systems* (MWSCAS), Springfield. MA. USA, 09-12, 2020.

[6]. Raulet M.A., Sixdenier F., Guinand B., Morel L., Goyet R., "Limits and rules of use of a dynamic flux tube model," *COMPEL.*, 27(1) :256 – 265, 2008.

[7]. A. T. Bui, F. Sixdenier, L. Morel, N. Burais, "Characterization and Modeling of a Current Transformer Working Under Thermal Stress," *IEEE Transactions on Magnetics*, 48, , 2600 - 2604, 2012.

[8]. Heidari H., Bonizzoni E., Gatti U., Maloberti F., "A cmos current-mode magnetic hall sensor with integrated front-end," *IEEE Trans. Circuits Syst. I Regul. Pap.*, 62:1270-1278, 2015.

[9]. A. Upadhyaya, D. Sarkar, A. B. Choudhury, D. Roy, "Performance analysis of a three-phase SISFCL with the variation of circuit parameters using jiles atherton hysteresis model," in *2nd International Conference on Control. Instrumentation. Energy & Communication (CIEC)*, 220-224, Kolkata, India, 2016.

[10]. Atef Lekdim, Fabien Sixdenier, Riccardo Scorretti, Adnan Grihe, "Reluctance Network Model of Open-Loop Hall-Effect Current Sensor for Circuit-Type Simulation Software Analyses," *IEEE Sensors Journal*, 1-10, 2022.

[11]. S. Fagerstrom, N. Bengiami, *Modelling and characterization of power electronics converters Using Matlab Tools*. MATLAB - A Fundamental Tool for Scientific Computing and Engineering Applications, 1, 133-165, 2012.